IL NUOVO CIMENTO **45 C** (2022) 71
DOI 10.1393/ncc/i2022-22071-2

COMMUNICATIONS: SIF Congress 2021

4π-periodic AC Josephson current through a reconstructed quantum spin Hall constriction

L. VIGLIOTTI(*)

Dipartimento di Fisica, Università degli Studi di Genova - Genova, Italy

received 29 January 2022

Summary. — We consider a Josephson junction based on a long constriction between the helical edges of a two-dimensional topological insulator, tunnel-coupled to two superconductors, pierced by a magnetic flux, and subjected to an external bias. We analyse the general case of a reconstructed constriction; namely, the two direction-conserving tunnel couplings may have different intensities. We show that our model, as in the absence of edge reconstruction, admits the occurrence of a 4π-periodic component in the AC Josephson current as a function of the magnetic flux. Such feature is robust in a wide range of parameters. A detailed discussion on the temperature dependence is also provided.

1. – Introduction

The last two decades of research in condensed matter physics have brought to the forefront quantum materials with non-trivial topology [1]. A main role in this context is played by the quantum spin Hall effect (QSHE), a topological phase of matter hosting a pair of helical one-dimensional metallic states [2-4]. Such states are topologically protected from elastic backscattering by time-reversal symmetry. Due to its properties, the QSHE appears as a promising playground for applications in spintronics, superconducting spintronics, and topological quantum computation [5-33]. In order to exploit the potential of the QSHE, nanostructuring is necessary. In this direction, narrow constrictions between the edges are attracting intense research activity, although a single experiment has so far been reported [27]. Moreover, at the theoretical level, a full characterisation of a hybrid setup consisting of superconducting elements and constrictions is still lacking, although, very recently, an anomalous Josephson current periodicity with respect to an external magnetic flux has been reported [34].

(*) E-mail: lucia.vigliotti@edu.unige.it

Creative Commons Attribution 4.0 License (https://creativecommons.org/licenses/by/4.0)

In this paper, we analyse a quantum spin Hall constriction, coupled to two superconductors (SCs), in the presence of a magnetic field and a bias. Moreover, we include the possibility of having edge reconstruction, namely, a spatial separation between the metallic channels with different spin. We calculate the Josephson AC current, whose anomalous 4π-periodicity in the magnetic flux has been proposed as a signature of the formation of the constriction [34]. We prove that the anomalous periodicity persists even in the presence of edge reconstruction. At the same time, we highlight new aspects and details that arise due to reconstruction.

This paper is organised as follows: in sect. **2** we describe the model, together with a nod to the calculation of the current; in sect. **3** we present and discuss our results; finally, sect. **4** is devoted to our conclusions.

2. – Model

In this section, the Josephson junction analysed in this work, and shown in fig. 1(a), is introduced one element at a time.

The main ingredient is a long and narrow helical constriction, located halfway in the two-dimensional topological insulator (2DTI) region that bridges the superconducting leads. The 2DTI sample has length L and width W, while the constriction has length ℓ ($\ell < L$, $\ell > k_F^{-1}$, with k_F the Fermi momentum) and width $w \ll W$. In the long direction, along either edge, a couple of helical, metallic states is present. Owing to spin-momentum locking, they can be determined by making use of two indices: $\rho = \pm 1$ denoting the right/left direction of propagation and $\tau = \pm 1$ standing for the upper/lower edge. The fermionic operator annihilating an electron at position x in the ρ, τ channel is denoted by $\hat{\psi}_{\rho\tau}(x)$. The Hamiltonian associated to the constriction is matricially

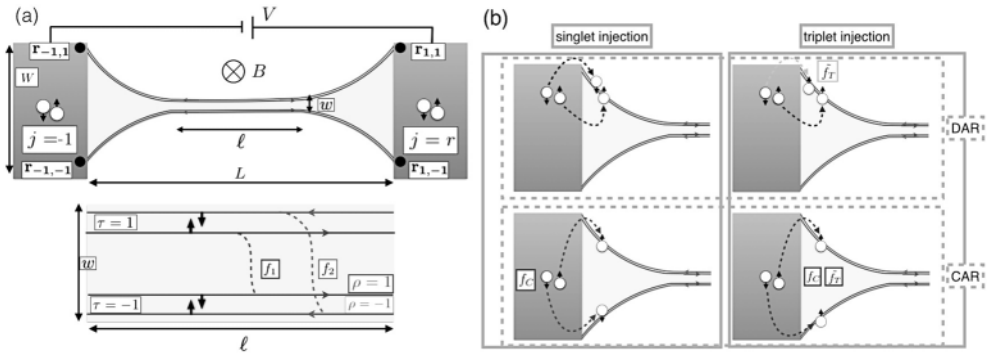

Fig. 1. – (a) Upper panel: schematic of the junction. A helical constriction of length ℓ and width w between two SCs (right, $j = 1$ and left, $j = -1$), halfway in a 2DTI sample of length L and width W. The tunnelling between the SCs and the upper ($\tau = 1$) and lower ($\tau = -1$) edge of the 2DTI takes place in the four contact points $\mathbf{r}_{j,\tau}$. The magnetic field B, applied perpendicularly to the plane of the junction, and the bias V are also shown. Lower panel: the direction-conserving couplings between the two edges are denoted by f_1 for the right-moving electrons ($\rho = 1$) and f_2 for the left-moving ones ($\rho = -1$). (b) Examples of tunnelling processes of a Cooper pair: in a spin-singlet or spin-triplet state (left/right panels) and either into the same edges or into different ones (upper/lower panels).

expressed by

(1)
$$\hat{H}_E^0 = \int_{-\infty}^{+\infty} \mathrm{d}x\, \hat{\psi}^\dagger(x) \begin{pmatrix} -i\hbar v_F \partial_x - \mu & 0 & 0 & f_1 \\ 0 & i\hbar v_F \partial_x - \mu & f_2 & 0 \\ 0 & f_2 & i\hbar v_F \partial_x - \mu & 0 \\ f_1 & 0 & 0 & -i\hbar v_F \partial_x - \mu \end{pmatrix} \hat{\psi}(x),$$

where $\hat{\boldsymbol{\psi}}(x) = (\hat{\psi}_{11}(x), \hat{\psi}_{-11}(x), \hat{\psi}_{-1-1}(x), \hat{\psi}_{1-1}(x))^T$. As throughout the paper we will consider long junctions and neglect any boundary effect, in eq. (1) we have taken the limit $L \to \infty$. The diagonal entries, with v_F the Fermi velocity and μ the chemical potential, represent the kinetic term. Two additional off-diagonal couplings, proportional to f_1 and f_2, are also present, and describe forward scattering processes. This kind of scattering events preserves the direction of motion of the electron, whereas the spin polarisation gets flipped as the electron moves from one edge to the other. f_1 is related to right-mover electrons and f_2 to left-mover ones (see fig. 1(a)). Allowing in principle the two couplings to take different values, we take into account a possible edge reconstruction of the constriction. This generalises the model inspected in [34], analysing it in a more experimentally realistic way. We mention in passing that, in the most general case, a backscattering contribution, under which the spin polarisation remains unchanged while the direction of motion is reversed, is present. However, since it is not relevant at all energy scales, it could be included perturbatively. Following [34], we keep the lowest perturbative order and neglect such processes.

Leveraging the limit $L \to \infty$, the Fourier transformation $\hat{\psi}_{\rho\tau}(x) = \frac{1}{\sqrt{L}} \sum_k \hat{c}_{k,\rho\tau}\, e^{ikx}$ permits a straightforward diagonalisation of eq. (1), leading to

$$\hat{H}_E^0 = \sum_{i=1}^{4} \sum_k E_{A_i}(k)\, \hat{A}_{k,i}^\dagger\, \hat{A}_{k,i}, \tag{2}$$

with

$$\hat{A}_{k,1} = \frac{1}{\sqrt{2}} \left(-\hat{c}_{k,-11} + \hat{c}_{k,-1-1}\right), \qquad E_{A_1}(k) = -f_2 - \hbar v_F k - \mu, \tag{3a}$$

$$\hat{A}_{k,2} = \frac{1}{\sqrt{2}} \left(\hat{c}_{k,-11} + \hat{c}_{k,-1-1}\right), \qquad E_{A_2}(k) = f_2 - \hbar v_F k - \mu, \tag{3b}$$

$$\hat{A}_{k,3} = \frac{1}{\sqrt{2}} \left(-\hat{c}_{k,11} + \hat{c}_{k,1-1}\right), \qquad E_{A_3}(k) = -f_1 + \hbar v_F k - \mu, \tag{3c}$$

$$\hat{A}_{k,4} = \frac{1}{\sqrt{2}} \left(\hat{c}_{k,11} + \hat{c}_{k,1-1}\right), \qquad E_{A_4}(k) = f_1 + \hbar v_F k - \mu. \tag{3d}$$

These new eigenstates are equal superpositions of an upper-edge state ($\hat{c}_{k,11}$, $\hat{c}_{k,-11}$) and a lower-edge state ($\hat{c}_{k,1-1}$, $\hat{c}_{k,-1-1}$), and have right ($\hat{A}_{k,3}$, $\hat{A}_{k,4}$) or left ($\hat{A}_{k,1}$, $\hat{A}_{k,2}$) chirality. The f_1/f_2 couplings split the two right-mover/left-mover branches in a way that resembles a spin-orbit coupling.

The constriction is tunnel-coupled on either side to a semi-infinite, three-dimensional SC, labelled by $j = -1$ (left SC) and $j = 1$ (right SC) and described by a standard BCS

Hamiltonian

$$\hat{H}_S^j = \frac{1}{2}\int \mathrm{d}\mathbf{r}\left(\hat{\Psi}^\dagger_{j,\uparrow}(\mathbf{r}),\hat{\Psi}^\dagger_{j,\downarrow}(\mathbf{r}),\hat{\Psi}_{j,\uparrow}(\mathbf{r}),\hat{\Psi}_{j,\downarrow}(\mathbf{r})\right)\mathcal{H}_S^j\begin{pmatrix}\hat{\Psi}_{j,\uparrow}(\mathbf{r})\\ \hat{\Psi}_{j,\downarrow}(\mathbf{r})\\ \hat{\Psi}^\dagger_{j,\uparrow}(\mathbf{r})\\ \hat{\Psi}^\dagger_{j,\downarrow}(\mathbf{r})\end{pmatrix}, \tag{4}$$

with

$$\mathcal{H}_S^j = \left(-\nabla^2_{\mathbf{r}} - \mu_{SC}\right)\alpha_z + i\Delta\left(e^{i\varphi_0^j}\,\frac{\alpha_x-\alpha_y}{2} - e^{-i\varphi_0^j}\,\frac{\alpha_x+\alpha_y}{2}\right)\sigma_y, \tag{5}$$

$\alpha_{x,y,z}$ and $\sigma_{x,y,z}$ being the Pauli matrices acting in the particle-hole and in the spin spaces, respectively, and $\hat{\Psi}_{j,\sigma}$, with $\sigma =\uparrow / \downarrow$ the spin polarisation, the fermionic operators in the j-th SC. The superconducting pairing is given by $\Delta\, e^{i\phi_0^j}$, and μ_{SC} is the chemical potential of both the SCs. The tunnelling at the interface with the constriction is ruled by the tunnelling Hamiltonian

$$\hat{H}_T^j = \int \mathrm{d}x \int \mathrm{d}\mathbf{r}\left(\hat{\Psi}^\dagger_{j,\uparrow},\hat{\Psi}^\dagger_{j,\downarrow}\right)\mathcal{T}^j(\mathbf{r},x)\begin{pmatrix}\hat{\psi}_{11}\\ \hat{\psi}_{-11}\\ \hat{\psi}_{-1-1}\\ \hat{\psi}_{1-1}\end{pmatrix} + h.c., \tag{6}$$

with

$$\mathcal{T}^j(\mathbf{r},x)_{\sigma,\rho\tau} = \frac{\mathfrak{T}}{\sqrt{1+f_T^2}}\,(if_T)^{\frac{1-\sigma\rho\tau}{2}}\,e^{i\rho k_F x}\,\delta\left(x - j\frac{L}{2}\right)\,\delta(\mathbf{r}-\mathbf{r}_{j,\tau}). \tag{7}$$

Here k_F is the Fermi momentum in the constriction, $\mathfrak{T}$ is the tunnelling coefficient associated with the opacity of the barrier and $f_T \ll 1$ is the ratio of spin-reversing processes over the spin-conserving ones. Such spin-flips are produced by the Rashba coupling of the material [35]. Moreover, the tunnelling injection is assumed to be point-like and to occur at the contact points between the j-th SC and the edges, denoted by $\mathbf{r}_{j,\tau}$ and marked in fig. 1(a).

We can integrate out the SCs in the energy regime $E \ll \Delta$ (which implies $k_BT,\, eV \ll \Delta$), and obtain an effective Hamiltonian for our system:

$$\hat{H}_E^0 + \sum_{j=\pm1}\left(\hat{H}_T^j + \hat{H}_S^j\right) \to \hat{H}_E^0 + \sum_{j=\pm1}\delta\hat{H}_E^j.$$

Here, $\delta\hat{H}_E^j$ keeps track of the effect of the j-th SC on the constriction, namely a tunneling of couples of electrons as Cooper pairs,

$$\delta\hat{H}_E^j \approx \sum_{\rho_1\tau_1,\rho_2\tau_2}\left[\Gamma_{\rho_1\tau_1,\rho_2\tau_2,j}\hat{\psi}_{\rho_1\tau_1}(x_j^-)\hat{\psi}_{\rho_2\tau_2}(x_j^+) + h.c.\right]. \tag{8}$$

From now on, for notational convenience, we will use $\zeta_1,\zeta_2 = \rho_1\tau_1,\rho_2\tau_2$. Two new variables $x_j^\pm$ have been introduced, $x_j^\pm = jL/2 \pm \delta_{\zeta,\zeta'}\xi/2$, with $\xi = \hbar v_F/\Delta$ the coherence

length in the edges, $\xi \ll L$. The splitting ξ allows processes with $\zeta_1 = \zeta_2$, otherwise forbidden by the Pauli principle.

Each addend of the sum represents a possible tunnelling process, whose features are encoded in the coefficients $\Gamma_{\zeta_1,\zeta_2,j}$, given by [34, 36]

$$\Gamma_{\zeta_1,\zeta_2,j} = (-1)^{\delta_{\zeta_1,-1-1}\delta_{\zeta_2,1-1}}\Gamma(\tilde{f}_T)^{\delta_{\rho_1*\tau_1,\rho_2*\tau_2}}(f_C)^{\delta_{\tau_1,-\tau_2}}e^{i[\frac{j}{2}k_F L(\rho_1+\rho_2)-\varphi_j^0]}, \tag{9}$$

where $\tilde{f}_T = f_T/\sqrt{1+f_T^2}$ while the quantity f_C arises from the integration of the SCs, $f_C \sim f(k_{F,S}W)e^{-W/\xi_S}$, with f an oscillatory and decaying function depending on the spatial dimension of the SCs, $k_{F,S}$ the Fermi momentum in the SCs and ξ_S their coherence length. Similarly to f_T for the spin-flips, f_C represents the ratio of crossed Andreev reflections or CAR (the electrons forming the Cooper pair are injected into or out of opposite edges) over direct Andreev reflections or DAR (the electrons forming the Cooper pair tunnel into or out of the same edge). Lastly, $\Gamma = \pi\mathfrak{T}^2 N_S$, with N_S the normal density of states per spin at the Fermi-level in the SCs, is the tunnelling rate. See fig. 1(b) for an overview.

Taking advantage of symmetries and multiplicities, the summation in eq. (8) can be reduced to the following terms:

$$\Gamma_{11,11,j},\ \Gamma_{11,-11,j},\ \Gamma_{11,-1-1,j},\ \Gamma_{11,1-1,j},\ \Gamma_{-11,-11,j},\ \Gamma_{-11,-1-1,j},\ \Gamma_{-11,1-1,j},$$
$$\Gamma_{-1-1,-1-1,j},\ \Gamma_{-1-1,1-1,j},\ \Gamma_{1-1,1-1,j}.$$

Following [34, 36, 37], we now insert the effects of the magnetic field, perpendicular to the constriction, and the bias V across the SCs.

Concerning the magnetic field, we neglect every effect apart from the Aharonov-Bohm phase. It can be shown that this is introduced only in the processes involving a direct Andreev reflection: $\gamma^{AB} = \pi\phi/\phi_0$ in the case of DAR and $\gamma^{AB} = 0$ in the case of CAR, with $\phi_0 = h/2e$ the superconducting flux quantum. On the other hand, the bias is responsible for a linear time dependence of the superconducting phase difference, proportional to $\omega_J = 2eV/\hbar$. Altogether, we have $\varphi_r - \varphi_l = (\varphi_r^0 - \varphi_l^0) + \gamma^{AB} + \omega_J t$. To take this into account, we modify the phase factor in eq. (9) as

$$e^{-i\varphi_j^0} \to e^{-i\left[\varphi_j^0 + j\frac{1}{2}\left(\omega_J t + \frac{\pi\phi\delta_{\tau_1,\tau_2}}{\phi_0}\right)\right]}. \tag{10}$$

Finally, we give a hint of the calculation of the current. All the details can be found in [34], with the additional subtlety of keeping f_1, f_2 distinguished.

The coupling to the SCs produces a net change in the number of electrons in the edges $\hat{N} = \sum_i \sum_k \hat{A}_{ki}^\dagger \hat{A}_{ki}$. We have $\dot{\hat{N}} = \dot{\hat{N}}^r + \dot{\hat{N}}^l$, with $\dot{\hat{N}}^j = i[\delta\hat{H}_E^j, \hat{N}]/\hbar$.

The operator $\hat{I}^j$, relative to the current flowing in the constriction, is given by $\hat{I}^j(t) = e\dot{\hat{N}}^j$, $e > 0$. More precisely, $\hat{I}^r(t)$ and $\hat{I}^l(t)$ are the currents injected from the right and left superconducting leads in the edges. The total current is given by $\hat{I}^{tot}(t) = \hat{I}^r(t) - \hat{I}^l(t)$.

Up to linear order in $\delta\hat{H}_E = \sum_j \delta\hat{H}_E^j$ (second order in the tunnelling rate Γ), we get

$$I^j(t) \approx \frac{i}{\hbar}\int_{-\infty}^{t} \mathrm{d}\tau \left\langle \left[\delta\hat{H}_E(\tau), \hat{I}^j(t)\right]\right\rangle_0. \tag{11}$$

The average is calculated with respect to the unperturbed system (described by $\hat{H}_E^0$, see eq. (2)) in the far past.

In the next section, the following dimensionless quantities will be employed: $\tilde{L} = \frac{L\Delta}{\hbar v_F}$, $\tilde{T} = \frac{\pi k_B T}{\Delta}$, $\tilde{V} = \frac{eV}{\Delta}$, $\tilde{\mu} = \frac{\mu}{\Delta}$, $\tilde{f}_{1/2} = \frac{f_{1/2}}{\Delta}$.

3. – Results and discussion

3˙1. *Anomalous 4π-periodicity.* – Developing the calculation sketched in the previous section, we obtain the following expression for the right current

(12)
$$I^r(t) = \mathcal{C}\,\mathrm{Im}\Bigg\{ e^{-i(\omega_J t + \varphi_r^0 - \varphi_l^0)} \int_0^{+\infty} ds\, e^{is\tilde{V}} \Bigg[A_1\left(\tilde{f}_1, \tilde{f}_2\right) \cos\left(\pi \frac{\phi}{\phi_0}\right) + A_2\left(\tilde{f}_1\right) \sin\left(\frac{\pi}{2}\frac{\phi}{\phi_0}\right) + A_3\left(\tilde{f}_1, \tilde{f}_2\right) \Bigg] \Bigg\},$$

with $s = t'\Delta/\hbar$, t' being a time variable, and $\mathcal{C} \equiv (-2e\Delta\Gamma^2)/(\pi^2\hbar^3 v_F^2)$. The left current $I^l(t)$ is obtained by conjugating the two complex exponentials and by exchanging $\tilde{f}_1$ and $\tilde{f}_2$.

We restrict our discussion to the current contribution that is aligned with the bias direction according to fig. 1(a), that is $I^r(t)$. Carrying out the integration, the full analytical expression for $\tilde{V} > 0$ is

(13)
$$I^r(t) = \mathcal{C}\,\mathrm{Im}\Bigg\{ e^{-i(\omega_J t + \varphi_r^0 - \varphi_l^0)} \left[\tilde{A}_1\left(\tilde{f}_1, \tilde{f}_2\right) \cos\left(\pi \tfrac{\phi}{\phi_0}\right) + \tilde{A}_2\left(\tilde{f}_1\right) \sin\left(\tfrac{\pi}{2}\tfrac{\phi}{\phi_0}\right) + \tilde{A}_3\left(\tilde{f}_1, \tilde{f}_2\right) \right] \Bigg\},$$

with

(14a)
$$\tilde{A}_1\left(\tilde{f}_1, \tilde{f}_2\right) = \frac{\pi}{6} \exp\left[-2\tilde{\mu} + \tilde{V}(-1 + i\tilde{L})\right] \Bigg\{ i \exp\left[i\left(2k_F L + 2\tilde{L}\tilde{\mu}\right)\right] \tilde{f}_T^2\, \tilde{V} \Bigg[6 + \left(-6 + 4\tilde{T}^2 + \tilde{V}^2\right) \times \cos\left(2\tilde{f}_1\right) + \left(4\tilde{T}^2 + \tilde{V}^2\right) \cosh\left(2\tilde{f}_1 - i2\tilde{f}_1\tilde{L}\right) \Bigg] + \frac{12\tilde{T}}{\sinh\left(2\tilde{L}\tilde{T}\right)} \cosh\left(\tilde{f}_1 - i\tilde{f}_1\tilde{L}\right) \times \cosh\left(\tilde{f}_2 + i\tilde{f}_2\tilde{L}\right) \Bigg\},$$

(14b)
$$\tilde{A}_2\left(\tilde{f}_1\right) = -\frac{\pi f_C \tilde{f}_T \tilde{V}}{6} \exp\left[i2k_F L + \left(-1 + i\tilde{L}\right)\left(\tilde{V} + 2\tilde{\mu}\right)\right] \left(-24 + 4\tilde{T}^2 + \tilde{V}^2\right) \sin\left(2\tilde{f}_1\right),$$

(14c)
$$\tilde{A}_3\left(\tilde{f}_1, \tilde{f}_2\right) = \frac{\pi}{6} \exp\left[-2\tilde{\mu} + \tilde{V}(-1 + i\tilde{L})\right] \Bigg\{ -i \exp\left[2ik_F L + 2i\tilde{L}\tilde{\mu}\right] \tilde{V} \Bigg[-6\left(f_C^2 - \tilde{f}_T^2\right) + \tilde{f}_T^2\left(-6 + 4\tilde{T}^2 + \tilde{V}^2\right) \cos\left(2\tilde{f}_1\right) - \tilde{f}_T^2\left(4\tilde{T}^2 + \tilde{V}^2\right) \cosh\left(2\tilde{f}_1 - 2i\tilde{f}_1\tilde{L}\right) \Bigg] + 6\frac{\tilde{T}}{\sinh\left(2\tilde{L}\tilde{T}\right)} \Bigg[\left(-1 + 2f_C^2\tilde{f}_T^2\right) \cosh\left(\tilde{f}_1 + \tilde{f}_2 - i\tilde{f}_1\tilde{L} + i\tilde{f}_2\tilde{L}\right) + \cosh\left(\tilde{f}_1 - \tilde{f}_2 - i\tilde{f}_1\tilde{L} - i\tilde{f}_2\tilde{L}\right) \Bigg] \Bigg\}.$$

TABLE I. – *Transport processes contributing to $I^r(t)$: the initial (after the tunnelling from the left SC to the edges) and final state (before the tunnelling from the edges to the right SC) of the Cooper pair are indicated, together with the $\tilde{A}_i$ coefficient they are associated with.*

$\tilde{A}_1$:	$u\uparrow u\uparrow\rightarrow u\uparrow u\uparrow$, $l\uparrow l\downarrow\rightarrow u\uparrow u\downarrow$,	$l\downarrow l\downarrow\rightarrow l\downarrow l\downarrow$, $u\uparrow u\downarrow\rightarrow l\uparrow l\downarrow$,	$u\uparrow u\uparrow\rightarrow l\downarrow l\downarrow$, $u\uparrow u\downarrow\rightarrow u\uparrow u\downarrow$,	$l\downarrow l\downarrow\rightarrow u\uparrow u\uparrow$, $l\uparrow l\downarrow\rightarrow l\uparrow l\downarrow$.
$\tilde{A}_2$:	$u\uparrow l\downarrow\rightarrow u\uparrow u\uparrow$,	$u\uparrow l\downarrow\rightarrow l\downarrow l\downarrow$,	$u\uparrow u\uparrow\rightarrow u\uparrow l\downarrow$,	$l\downarrow l\downarrow\rightarrow u\uparrow l\downarrow$.
$\tilde{A}_3$:	$u\downarrow l\downarrow\rightarrow u\downarrow l\downarrow$, $u\uparrow l\downarrow\rightarrow u\uparrow l\downarrow$.	$u\uparrow l\uparrow\rightarrow u\uparrow l\uparrow$,	$u\downarrow l\downarrow\rightarrow u\uparrow l\uparrow$,	$u\uparrow l\uparrow\rightarrow u\downarrow l\downarrow$,

The explicit form of $I^l(t)$ is not reported.

The different scattering processes contributing to the current can be singled out. Table I lists all the processes giving a nonzero contribution to $I^r(t)$, specifying the coefficient $\tilde{A}_i$ they contribute to.

Equation (13) shows that a term with a 4π-periodicity on the magnetic flux ϕ is present even if the constriction is reconstructed, as emerged in [34] for the non-reconstructed case. This means that the anomalous periodicity is not related to the particular restriction $\tilde{f}_1 = \tilde{f}_2$. The addend of interest is proportional to $\tilde{A}_2$ and depends, for each current, on one single tunnelling coefficient: the right-mover coefficient $\tilde{f}_1$ in the case of $I^r(t)$ and the left-mover coefficient $\tilde{f}_2$ in the case of $I^l(t)$. Given $\tilde{f}_1$ and $\tilde{f}_2$, the relative weight of the 4π-component in the two currents is hence different, meaning that, in principle, it may exhibit a less or worse visibility in $I^r(t)$ and $I^l(t)$. Moreover, looking for instance at $I^r(t)$, since $\tilde{A}_2 \propto f_C \tilde{f}_T \sin(2\tilde{f}_1)$ we also recover the necessity of f_C, $\tilde{f}_T \neq 0$, as in [34].

We have thereby shown that, while without reconstruction what is needed is $\tilde{f}_1 = \tilde{f}_2 \equiv \tilde{f} \neq 0$, in our present analysis a single coupling is sufficient.

To better illustrate our finding, as in [34,36], the quantity we will consider is the ω_J-Fourier component of $I^r(t)$, given by $I^r_{\omega_J} = |1/T \int_{-\mathrm{T}/2}^{\mathrm{T}/2} \mathrm{d}t\, e^{-i\omega_J t} I^r(t)|$, where $\mathrm{T} = 2\pi/\omega_J$. We obtain

$$I^r_{\omega_J} = \left| \mathcal{C} \left[\tilde{A}_1\left(\tilde{f}_1, \tilde{f}_2\right) \cos\left(\pi \frac{\phi}{\phi_0}\right) + \tilde{A}_2\left(\tilde{f}_1\right) \sin\left(\frac{\pi}{2}\frac{\phi}{\phi_0}\right) + \tilde{A}_3\left(\tilde{f}_1, \tilde{f}_2\right) \right] \right|. \tag{15}$$

We also find $I^l_{\omega_J} = I^r_{\omega_J}$, provided that $\tilde{f}_1$ and $\tilde{f}_2$ are interchanged in $\tilde{A}_{1/2/3}$ and that the bias is reversed, $\tilde{V} \to -\tilde{V}$.

Figure 2 shows $I^r_{\omega_J}$ for some specific values of the tunnelling coefficients and at a fixed temperature $\tilde{T} = 0.1$. It is clearly visible that, whenever $\tilde{f}_1 = 0$, a standard 2π-periodicity is recovered (see dashed and dotted lines), while all the other cases, either with edge reconstruction (including $\tilde{f}_2 = 0$) or not, exhibit the 4π-feature.

3˙2. *Interference pattern and temperature dependence.* – So far, we have discussed the occurrence of the 4π-signature, which is not affected by the edge reconstruction. On the other hand, the visibility of the feature depends on which one among the differently periodic terms dominates; this is related to both $\tilde{f}_1$ and $\tilde{f}_2$ and is, therefore, sensitive to the edge reconstruction. To better appreciate the relevance of the different periodicity,

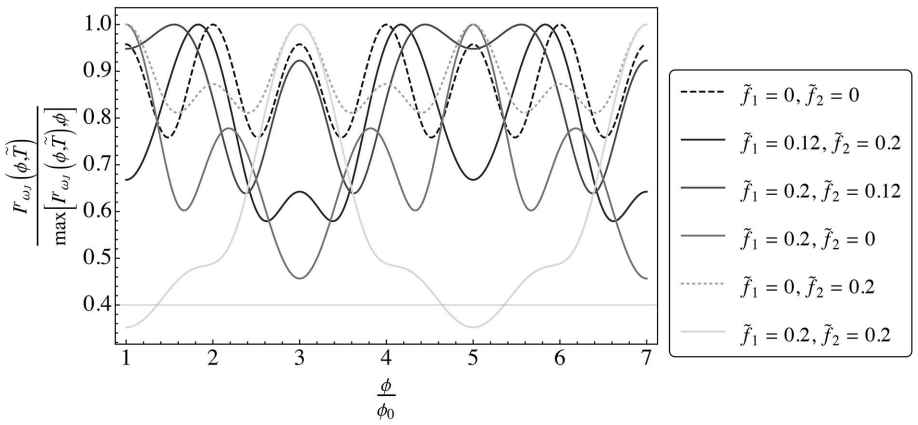

Fig. 2. – $I^r_{\omega_J}$, normalised with respect to its maximum, for $\tilde{L} = 20$, $k_F L = 6\pi$, $\tilde{f}_T = 0.4$, $f_C = 0.3$, $\tilde{\mu} = 0.0001$, $\tilde{T} = 0.1$ and $\tilde{V} = 0.1$, as a function of ϕ (in units of ϕ_0). The different curves correspond to different values of $\tilde{f}_1$, $\tilde{f}_2$. It is visible that whenever $\tilde{f}_1 = 0$, a standard 2π-periodicity is recovered (dashed and dotted lines), while in all the other cases, either in the presence of edge reconstruction or not, and regardless of the value of $\tilde{f}_2$, $I^r_{\omega_J}$ is 4π-periodic.

since eq. (15) contains several interfering terms, we rewrite it conveniently as

$$I^r_{\omega_J} = |\mathcal{C}|\sqrt{\alpha + \beta\cos\left(2\pi\frac{\phi}{\phi_0}\right) + \gamma\sin\left(\frac{3\pi}{2}\frac{\phi}{\phi_0}\right) + \delta\cos\left(\pi\frac{\phi}{\phi_0}\right) + \epsilon\sin\left(\frac{\pi}{2}\frac{\phi}{\phi_0}\right)}, \tag{16}$$

where

$$\alpha = \frac{|\tilde{A}_1|^2}{2} + \frac{|\tilde{A}_2|^2}{2} + |\tilde{A}_3|^2, \qquad \beta = \frac{|\tilde{A}_1|^2}{2}, \qquad \gamma = \mathrm{Re}\tilde{A}_1\mathrm{Re}\tilde{A}_2 + \mathrm{Im}\tilde{A}_1\mathrm{Im}\tilde{A}_2,$$
$$\delta = -\frac{|\tilde{A}_2|^2}{2} + 2\mathrm{Re}\tilde{A}_1\mathrm{Re}\tilde{A}_3 + 2\mathrm{Im}\tilde{A}_1\mathrm{Im}\tilde{A}_3,$$
$$\epsilon = 2\mathrm{Re}\tilde{A}_2\mathrm{Re}\tilde{A}_3 + 2\mathrm{Im}\tilde{A}_2\mathrm{Im}\tilde{A}_3 - \mathrm{Re}\tilde{A}_1\mathrm{Re}\tilde{A}_2 - \mathrm{Im}\tilde{A}_1\mathrm{Im}\tilde{A}_2.$$

This makes evident that interference plays a crucial role in the system we analyse: although the processes at the root of the 4π-periodicity (those contributing to $\tilde{A}_2$, see table I) are just a few, they are related to all the others through the interference pattern. The resulting periodicity is driven by the coefficients β, γ, δ, ϵ, while α is a flux-independent offset. We focus on their dependence on temperature, since in [34] it was pointed out that at high temperature some challenges arise.

Given $\tilde{f}_1$, $\tilde{f}_2$, all the coefficients exhibit a high sensitivity to temperature in the low-temperature regime and up to $\tilde{T} \simeq 0.12$, as shown in figs. 3(a), (b), while in the high-temperature regime we can inspect (spanning up to $\tilde{T} \simeq 0.25$), their variation becomes slower. At high temperature, the offset α is always steadily set to a finite value: see again both figs. 3(a), (b), where we considered $\tilde{f}_1 = 0.12$, $\tilde{f}_2 = 0.2$ and viceversa, respectively. Concerning the prefactors of the flux-dependent terms β, γ and ϵ, either they approach zero, or they settle to very small values if compared to α. On the other hand, δ behaves differently: either it increases with temperature, as in fig. 3(c), or it reaches a plateau

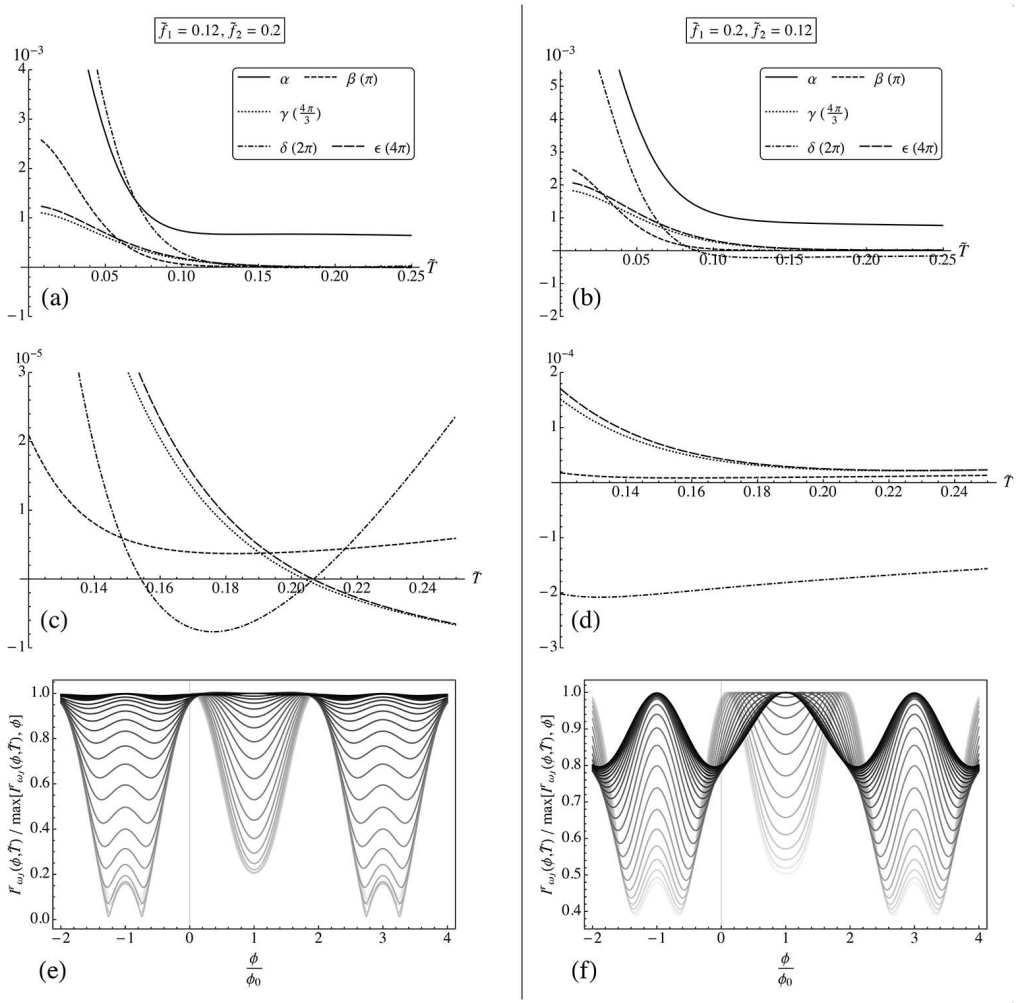

Fig. 3. – (a), (b): temperature dependence of the coefficients α, β, γ, δ, ϵ, for $\tilde{T}$ varying between 0.008 and 0.25. The legend specifies to which periodicity each coefficient corresponds to. (c), (d): zoom of (a), (b) on the high-temperature range, from $\tilde{T} = 0.12$ to $\tilde{T} = 0.25$, only for the prefactors of the flux-dependent terms β, γ, δ and ϵ. (e), (f): $I^r_{\omega_J}$, normalised with respect to its maximum, as a function of ϕ (in units of ϕ_0) and for $\tilde{T}$ varying between 0.008 (lighter grey) and 0.2 (darker grey) with steps of 0.008. Plots (a), (c), (e) correspond to $\tilde{f}_1 = 0.12$, $\tilde{f}_2 = 0.2$, while plots (b), (d), (f) to the viceversa. In all cases, $\tilde{L} = 20$, $k_F L = 6\pi$, $\tilde{f}_T = 0.4$, $f_C = 0.3$, $\tilde{\mu} = 0.0001$ and $\tilde{V} = 0.1$.

with value significantly greater in magnitude than the others, as in fig. 3(d). In the first case it is possible for the 4π-periodicity to persist at high temperature, since the different periodicities have comparable weight (fig. 3(e)). However, this weight being small, the curves are flattened and their peak structure weakened. In contrast, in the second case the 2π-periodic contribution becomes sharply dominant and the 4π-periodic one almost invisible (fig. 3(f)). This analysis substantiates and gives a mathematical explanation

to two statements of [34] about the high-temperature regime: firstly, the incidence of the 4π-periodicity of $I^r_{\omega_J}$ is worsened, while at low temperature it is always noticeable; secondly, overall its intensity (namely, the peak-to-peak distance) drops down. All these remarks are valid for any $\tilde{f}_1$, $\tilde{f}_2$, even if they are equal.

We can now leverage our comment below eq. (15): since $I^r_{\omega_J}$ computed for $\tilde{V} > 0$ and $I^l_{\omega_J}$ computed for $\tilde{V} < 0$ have a different insight of the tunnelling processes, in principle they might display more or less evidently the 4π-periodicity at high temperature. This is very well visible comparing fig. 3(e) and fig. 3(f), that we can interpret respectively as $I^r_{\omega_J}$ for $\tilde{V} > 0$ and $I^l_{\omega_J}$ for $\tilde{V} < 0$ of a constriction with $\tilde{f}_1 = 0.12$, $\tilde{f}_2 = 0.2$. This connection between the two measures offers a doubled possibility of inspection of the anomalous periodicity that can all rely on the analytical results at the beginning of the section. It mostly comes in handy if one of the tunnelling coefficients is zero and therefore only one of the currents is 4π-periodic.

4. – Conclusions

We have considered a Josephson junction where the non-superconducting element is represented by a reconstructed constriction between helical edge states. We have shown that the 4π-periodicity in the piercing flux, predicted in the absence of reconstruction, is still present. We have then assessed its visibility by giving analytical expressions that are remarkably simpler than the ones previously reported, which also greatly facilitate the physical interpretation in terms of interference effects.

Furthermore, inspecting the dependence on temperature, we have found substantial agreement with [34] about the low visibility of the 4π-periodicity at high temperature, but also revealed further remarks that may lessen the difficulty. To this regard, in particular, we have pointed out a relation between the right and left currents in the presence of opposite bias, showing that this offers an additional way to recognise the signature.

* * *

The author acknowledges Niccolò Traverso Ziani and Maura Sassetti for their contribution to the topic presented in this paper. This work was supported by the "Dipartimento di Eccellenza MIUR 2018-2022".

REFERENCES

[1] König M. *et al.*, *Science*, **318** (2007) 766.
[2] Qi X.-L. and Zhang S.-C., *Rev. Mod. Phys.*, **83** (2011) 1057.
[3] Bernevig B. A. *et al.*, *Science*, **314** (2006) 1757.
[4] Hasan M. Z. and Kane C. L., *Rev. Mod. Phys.*, **82** (2010) 3045.
[5] Kane C. L. and Mele E. J., *Phys. Rev. Lett*, **95** (2005) 226801.
[6] Kane C. L. and Mele E. J., *Phys. Rev. Lett*, **95** (2005) 146802.
[7] Qi X.-L. *et al.*, *Nat. Phys.*, **4** (2008) 273.
[8] Fu L. and Kane C. L., *Phys. Rev. B*, **79** (2009) 161408(R).
[9] Knez I. *et al.*, *Phys. Rev. Lett.*, **107** (2011) 136603.
[10] Väyrynen J. I. and Ojanen T., *Phys. Rev. Lett.*, **107** (2011) 166804.
[11] Blasi A. *et al.*, *New J. Phys.*, **14** (2012) 013060.
[12] Dolcetto G. *et al.*, *Phys. Status Solidi (RRL)*, **7** (2013) 1059.
[13] Dolcetto G. *et al.*, *Phys. Rev. B*, **87** (2013) 235423.
[14] Ronetti F. *et al.*, *Phys. Rev. B*, **93** (2016) 165414.
[15] Hart S. *et al.*, *Nat. Phys.*, **10** (2014) 638.

[16] Linder J. and Robinson J. W. A., *Nat. Phys.*, **11** (2015) 307.
[17] Li J. *et al.*, *Phys. Rev. Lett.*, **117** (2016) 046804.
[18] Cayao J. and Black-Schaffer A. M., *Phys. Rev. B*, **96** (2017) 155426.
[19] Reis F. *et al.*, *Science*, **357** (2017) 287.
[20] Bocquillon E. *et al.*, *Nat. Nanotechnol.*, **12** (2017) 137.
[21] Traverso Ziani N. *et al.*, *Phys. Rev. B*, **95** (2017) 205418.
[22] Wu S. *et al.*, *Science*, **359** (2018) 76.
[23] Breunig D. *et al.*, *Phys. Rev. Lett.*, **120** (2018) 037701.
[24] Fleckenstein C. *et al.*, *Phys. Rev. Lett.*, **122** (2019) 066801.
[25] Traverso Ziani N. *et al.*, *Phys. Rev. B*, **101** (2020) 195303.
[26] Keidel F. *et al.*, *Phys. Rev. Res.*, **2** (2020) 022019.
[27] Strunz J. *et al.*, *Nat. Phys.*, **16** (2020) 83.
[28] Fleckenstein C. *et al.*, *Phys. Rev. B*, **103** (2021) 125303.
[29] Ronetti F. *et al.*, *Phys. Rev. Res.*, **2** (2020) 013203.
[30] Blasi G. *et al.*, *Phys. Rev. Lett.*, **124** (2020) 227701.
[31] Ronetti F. *et al.*, *Phys. Rev. B*, **95** (2017) 115412.
[32] Acciai M. *et al.*, *Phys. Rev. B*, **98** (2018) 035426.
[33] Bours L. *et al.*, *Phys. Rev. Appl.*, **10** (2018) 014027.
[34] Vigliotti L. *et al.*, *New J. Phys.*, **24** (2022) 053017.
[35] Streda P. and Seba P., *Phys. Rev. Lett.*, **90** (2003) 256601.
[36] Galambos T. H. *et al.*, *Phys. Rev. Lett.*, **125** (2020) 157701.
[37] Tkachov G. *et al.*, *Phys. Rev. B*, **92** (2015) 045408.